



New low-cost, flow-through carbon electrodes characterized in brackish water

Arman Molaei¹ · Fareed Ahmed¹ · Ujwala Ail¹ · Xavier Crispin¹

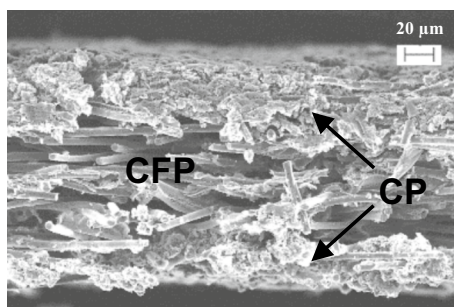
Received: 13 September 2022 / Accepted: 19 November 2022 / Published online: 7 December 2022
© The Author(s) 2022

Abstract

We propose a simple and low-cost flow-through electrode for electrochemical cells used for instance in capacitive desalination. We have coated macro-porous carbon fiber papers with various loads of carbon microporous particles to combine both a high surface area and an open structure for good fluid dynamics. In this first study, we restrict our investigation to the charging/discharging behavior, the identification of side reactions, and the effect of geometry on the diffusion of ions. The electrochemical performance was first investigated by cyclic voltammetry and galvanic charge–discharge techniques. The specific capacitance increases by three orders of magnitude upon adding the carbon particles. Then, electrochemical impedance spectroscopy revealed the presence of charge transfer phenomena and modification in the mass transport by the diffusion process for the coated electrode.

Graphical abstract

SEM image of the surface morphology of the cross section of CP/CFP/CP structure of the flow-through electrode.



Keywords Flow-through electrode · Desalination · Supercapacitors · Carbon fiber paper · And Carbon paste

Introduction

Carbon materials are crucial in the electrode composition utilized in energy storage/conversion devices owing to their unique combination of properties: large surface area of nanostructures, high mechanical strength, good electrical conductivity, acceptable chemical stability, and low-cost

(Porada et al. 2013; Zhang et al. 2018; Chander and Mangal 2019). Electrodes in supercapacitors and batteries are typically partially composed of carbon nano-materials such as carbon nanotubes, graphenes, and its oxides, ordered mesoporous carbons, activated carbons, and carbon blacks (Chander and Mangal 2019). Micro- and meso-porous electrodes (pore size < 2 nm and < 50 nm) are appropriate for charge storage as characterized by a large capacitance; however, they are typically not designed for flow electrochemical cells where the fluid should pass through the cells or through the macro-porous electrodes (Chander and Mangal 2019; Olabi et al. 2022).

✉ Arman Molaei
Arman.Molaei@liu.se

¹ Laboratory of Organic Electronics, Department of Science and Technology, Linköping University, 601 74 Norrköping, Sweden

Nowadays, there is a renewed interest in designing carbon-based electrodes for flow electrochemical cells because of the increasing demand for emerging key technologies such as capacitive desalination, redox flow batteries, and electrolyzers (Olabi et al. 2022; Elisadiki and King'ondeu 2020; Alkhadra et al. 2022). Electrolyzers are used to produce fuels and chemicals, as well as flow reactors in organic synthesis (Alkhadra et al. 2022). A flow electrochemical cell is typically composed of two carbon-based electrodes in contact with a positively and a negatively charge collector. The two electrodes are either sandwiching an ionic selective membrane separating the electrolyte on both sides, such as in redox flow batteries or by a polymer mesh (e.g., turbulence promoters (Bengoa et al. 1997)) to have the same liquid in contact with both electrodes, such as in some flow reactors (Mo et al. 2020). The flow of liquid can either pass by electrodes (flow-by, Fig. 1a) or through electrodes (flow-through, Fig. 1c). Both planar and porous electrodes can be used in the flow-by architecture (Fig. 1a, b). The functionality of the flow electrochemical cell depends on the physical and chemical properties of the electrode material. The electrode material can include an electrocatalyst that provides the specificity and the efficiency to the electron transfer reaction between the electrode and the reactant in the liquid. However, other parameters are important too, such as the flow rate of the electrolyte, the reactant mass transport, and the ionic and electronic currents in porous electrodes (Bengoa et al. 1997). Hence, the porosity and the morphology of the carbon electrode are crucial and impact the electrochemical performance in energy applications or chemical production (Mo et al. 2020; Rivera et al. 2015; Suss et al. 2012).

The density of the electrode and the type of porosity also play a role. Electrodes with high porosity but small pores have a high surface area ($\sim 1000 \text{ m}^2 \text{ g}^{-1}$), thus promoting any interfacial phenomena (electric double layer formation and electron transfer reaction), but they possess high fluid resistance (Fig. 1d). Because those electrodes can function in the flow-by architecture (Fig. 1b) but not in the flow-through cell (Fig. 1c). To ensure low fluid resistance for the flow-through geometry cell, open and macroscopic porosity with large pores offered by carbon clothes and carbon papers made of carbon fibers are typically used (Rivera et al. 2015) (Fig. 1f). The surface area is however much limited ($\sim 10 \text{ m}^2 \text{ g}^{-1}$) thus leading to low faradaic current density and low capacitance (Suss et al. 2012). There is a large interest in the development of the flow-through electrode architecture utilizing multi-scale porous electrodes (Suss et al. 2012) combining low fluid resistance and large surface area (Fig. 1e). A first strategy to increase the surface area was to chemically etch the surface of the carbon fibers (Zhang et al. 2013). In a second approach, nanorods have been grown on carbon fibers (Abbas et al. 2018). Recently, a third strategy was to use nanofibers of carbon created by the electrospinning

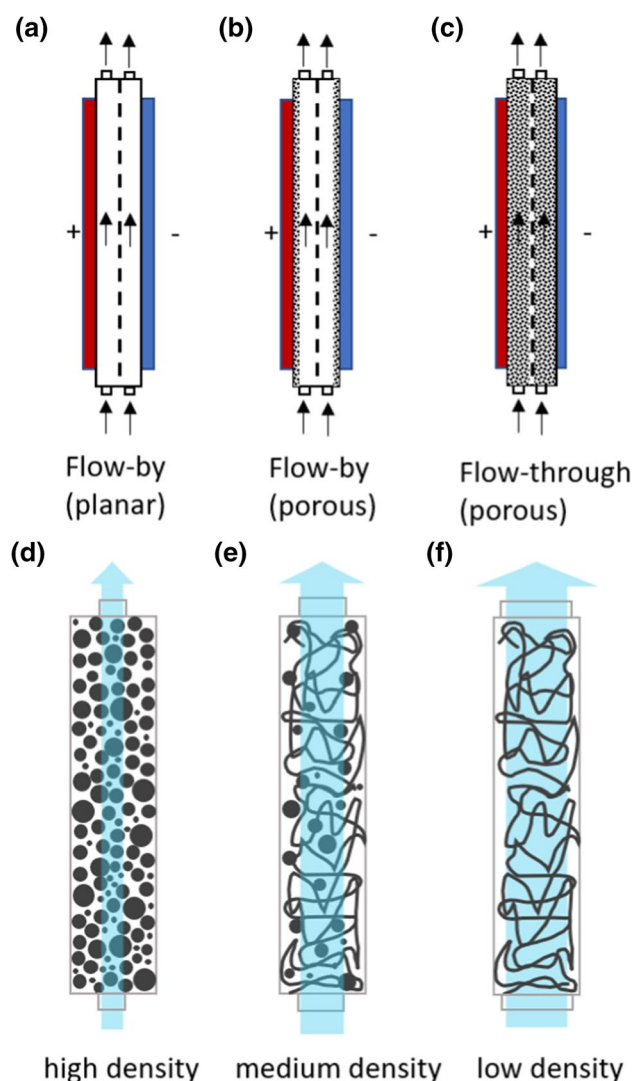


Fig. 1 The schematic of flow electrochemical cell: **a** planar and **b** porous flow-by cell and **c** porous flow-through cell constituted of **d** coated paste of porous carbon nanoparticles CP, **e** multi-scale porous-coated carbon fiber (studied design), and **f** carbon fiber paper electrodes CFP

technique of a polymer before the pyrolysis ($700 \text{ m}^2 \text{ g}^{-1}$) (Ribadeneyra et al. 2020).

The charging of a planar and a porous electrode can be different and these differences are exalted for small pores and thick electrodes. Indeed, the transport of ions inside the porosity of the electrode deviates from the ionic transport found in the bulk of a solution. Ions need to follow convection paths in the porosity that reduces the effective diffusion length (Epstein 1989) and couple to the tortuosity factor of the electrode. Importantly, it is not an easy task to measure the diffusion of ions in a porous electrode mostly because the electronic conductivity of the electrode materials introduces various screening effects that prevent the use of spectroscopic methods. One technique that has been

developed is impedance spectroscopy which measures the complex impedance of the electrode in an electrolyte by applying a small AC bias in a range of frequencies to probe various phenomena taking place at different timescales. If electronic and ionic transports are not occurring at the same rate, this method enables to distinguish between those effects in the time domain. The physical interpretation of impedance spectra, i.e., the complex impedance versus frequency, requires the use of specific equivalent circuit models to represent each of the physical phenomena taking place insight the porous electrode. We can see a porous electrode as an assembly of pores connected ionically and electronically. In the simplest model, each pore could possess an ionic resistance, an electronic resistance as well as an electric double layer capacitor. This description is the basis for the so-called transmission line model (TLM) where a porous electrode is modeled by an assembly of serial resistors and branching capacitors (Tröltzsch and Kanoun 2012). In practice, ideal electrical elements such as resistors and capacitors cannot represent the flora of nonlinear phenomena taking place in electrochemistry even for the non-porous surface, such as the mass transport in a liquid modeled by a Warburg element; or the presence of boundaries that requires constant phase element (CPE) or charge transfer faradic reaction taking place at the electrode–electrolyte interface which can be approximated by a resistance (R_{CT}) (Volonino et al. 1992). Those phenomena introduce a degree of complexity where non-ideal electrical elements are necessary for making sense of the results (Elgrishi et al. 2018). Going deeper, theoretical modeling coupled to impedance spectroscopy enables to reveal various hidden effects such as the impact of the shape and the size of the pores on the impedance spectrum (Cooper et al. 2017).

Another tool revealing unique phenomena taking place in porous carbon electrodes is the theoretical modeling using advanced quantum chemical models or molecular dynamics. It enables for instance to access the diffusion of ions inside the pores (Pean et al. 2015). Three phenomena explain the high specific capacitance found for microporous carbon electrodes beside the simple argument of the effective surface area of the electrode (Chmiola et al. 2006): (i) The overscreening, found in the solution as a damped oscillation of the ion concentration (Fedorov and Kornyshev 2008), disappears inside the nano-porous electrode; and (ii) the conducting walls of pores screen efficiently the repulsion between ions in the electric double layer and promote a high interface charge density (Merlet et al. 2012); (iii) finally, the partial desolvation of ions in a pore results in a close distance between the electronic charge on the electrode and the ionic layer, which consequently increase the capacitance (Eijkelkamp et al. 2013).

In this work, we propose a new design for a flow-through electrode by coating a layer of high density paste of porous

carbon nanoparticles (CP) (Fig. 1d) onto the two sides of a low-density carbon fiber paper electrode (CFP) (Fig. 1f) to achieve the morphology depicted in Fig. 1e. This architecture keeps a high flow resistance in the middle of the CFP while increasing by several orders of magnitude the surface area of the electrode with the CP layer. In this article, we characterize these electrodes in a symmetric device without the effect of fluid dynamics. Instead, we focus on the understanding and electrochemical characterization of phenomena taking place in that microporous electrode and the interpretation of impedance spectroscopy data. NaCl added in the aqueous electrolyte was selected to relate this study to one of the potential applications: capacitive deionization (CDI), but in a forthcoming study, we will also explore its potential in electrolyzers.

Experimental section

Preparation of carbon particle CP electrode

A CP slurry was prepared by mixing predetermined amounts of Ketjen black nano-powder (KB, EC-600JD conductive carbon black, pore volume of 480–510 ml 100 g⁻¹, BET of 1400 m² g⁻¹, Akzo Nobel) as a conductive agent and activated carbon nano-powder (AC, pore volume of 0.7 ml g⁻¹, BET of 1600 m² g⁻¹, Kuraray) as a capacitive agent. The dry mass ratio of the KB and AC was 1:1. The mixture was then combined with a 14 wt% binder system made of CMC (Carboxymethylated cellulose, viscosity of 1500–3000 cP, Sigma-Aldrich) with SBR (Styrene butadiene rubber, viscosity of 50–250 mPa s, Sigma-Aldrich) in water. The resulting slurry was homogenized with a disperser (IKA T-25 digital Ultra-Turrax) at a high shear rate for 3 min. This homogenization process was repeated three times with the addition of water in each step to decrease the viscosity of the slurry. Each bare hydrophobic carbon fiber CFP substrate (AvCarb MGL190, porosity of 78%, density of 0.44 g cm⁻³, FuelCell-Store) was cut in the dimension of 3 × 7 cm² with a thickness of 0.019 cm and coated by the various amounts of CP slurry. The prepared CP-coated CFP electrode was dried in an oven at 60 °C for 2 h. The weight of each CP-coated CFP electrode was subtracted with the weight of bare CFP substrate to obtain the dried weight of the CP coating in successive steps of 0.003, 0.07, 0.013, 0.025, 0.05, 0.08, 0.1, and 0.16 g using a microanalytical balance (KERN ABJ-NM, Fisher Brand). Bare hydrophilic CFP substrates were prepared by immersing bare hydrophobic CFP substrates in 0.1 M H₂SO₄ solution for 10 min followed by rinsing with water and used for comparison. The morphology of the bare and CP-coated CFP electrodes were observed by using scanning electron microscopy (SEM, Zeiss Sigma 500 Gemini).

Cell preparation and electrochemical characterization

In the symmetrical configuration of CDI, two identical electrodes were prepared as the cathode and anode. Those identical electrodes were assembled by using a separator (Celgard 5550, microporous monolayer Polypropylene membrane, thickness of 110 μm , porosity of 55%) in 0.1 M NaCl electrolyte solution with a 7 ml total quantity. At the concentration considered of 0.1 M NaCl, the salty solution can also be classified as brackish water (0.03–0.42 M) (Zhang et al. 2018). An experimental electrochemical cell with the two flow-through CFP-CP electrodes was built according to the following architecture: end plastic plate/CFP-CP/separator/CFP-CP/end plastic plate inserted in a rectangular space next to a reservoir for inserting probes in the dimension of $2.6 \times 7.8 \times 0.6 \text{ cm}^3$. Cyclic voltammetry (CV), galvanostatic charge–discharge (GCD), and electrochemical impedance spectroscopy (EIS) were performed with an Autolab (SP-200) potentiostat/galvanostat coupled to a computer using EC-Lab software at room temperature. CV tests were carried out at the scanning rate of 5 mV s^{-1} within the potential range of 0–1 V if not otherwise stated. GCD experiments were carried out at the current density of 15 mA within the same potential range. EIS measurements were investigated at open-circuit voltage over a frequency range from 100 to 200 kHz with an AC voltage amplitude of 5 mV. Validity of EIS measurements (linear Kramers–Kronig tests) and modeling of EIS measurements were performed using RelaxIS 3 software developed by RHD instruments. All curves for CV, GCD, and EIS experiments were plotted at the second cycle to reach an equilibrium condition.

Results and discussion

The surface morphology of bare and CP-coated CFP electrodes is visualized by using SEM. A rich fibrous and microporous morphology of the bare CFP with an average fiber diameter of $5.2 \mu\text{m}$ is observable in Fig. 2a. This microstructure offers the possibility for low fluid resistance of the electrolyte but low capacitance (surface area). Applying the CP slurry on both sides of the CFP substrate makes a surface coating layer relatively compact with nano- and meso-pores due to the porosity of carbon particles (Fig. 2b). It is also obvious there is a good penetration of CPs into the CFP substrate. The appearance of cracks is mostly related to the shrinkage of the CP layer after the drying process improving the capillary property of the electrolyte inside of the electrode (Alkhadra et al. 2022). In this case, the presence of cracks is not necessarily a disadvantage since it enables liquid flow also across the electrode. Despite those cracks, the polymer binder CMC/SBR (Zhang et al. 2018) fills its role

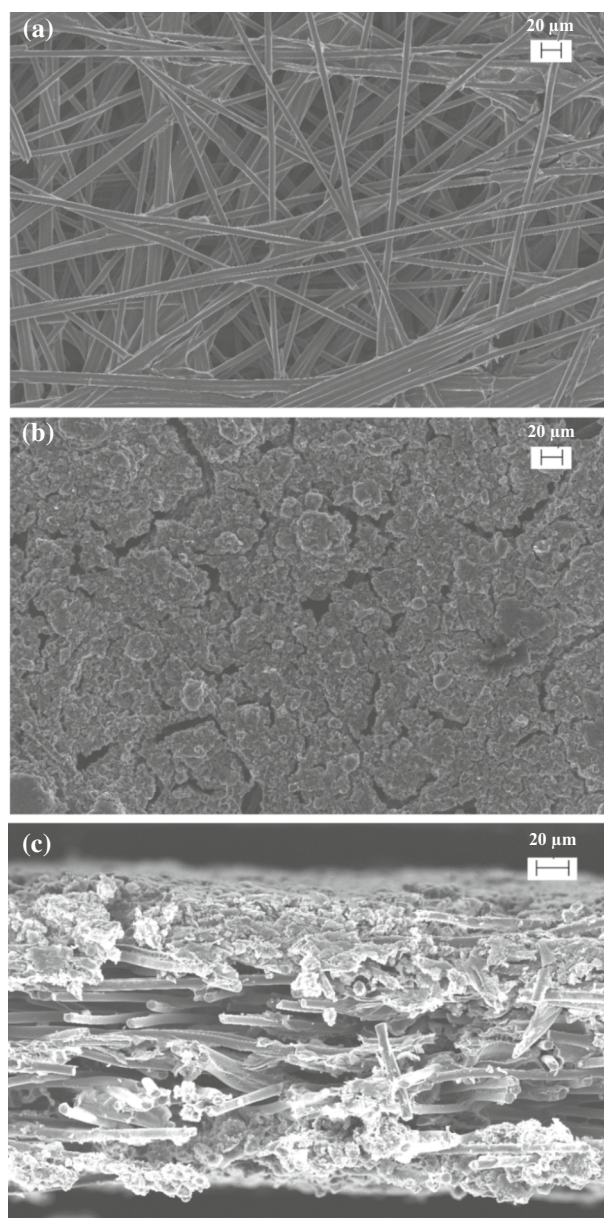


Fig. 2 SEM image of the surface morphology of **a** bare CFP, **b** 0.16 g CP-coated CFP electrode, and **c** the cross section of CP/CFP/CP structure of the flow-through electrode

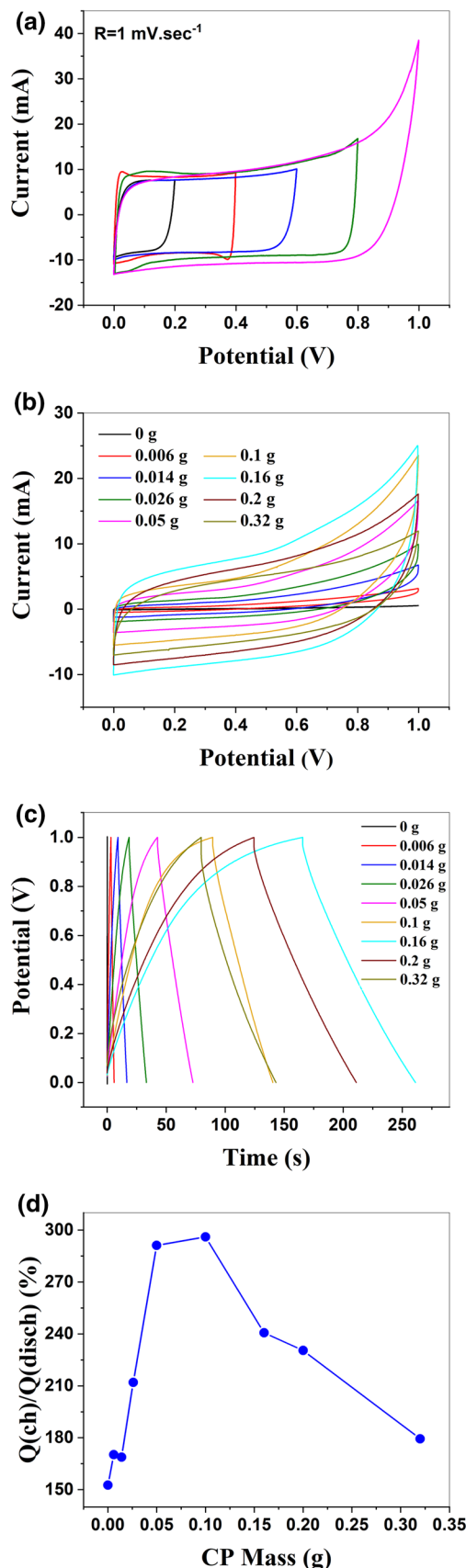
as no particle fall off the electrode by the touch of the finger and that the CP layer has good adhesion on the 3D scaffold of the CFP substrate. A cross-sectional image displays a double-layered structure with CP layers of approximately $20 \mu\text{m}$ in thickness that cover both sides of the microporous CFP to form a CP/CFP/CP structure (Fig. 2c). The use of two CP layers on the CFP substrate enables to load a high mass of carbon particles while keeping a good adhesion to the substrate. This design form of a robust and high capacitance flow-through electrode. This prepared structure combines a large and accessible surface area with desirable pore

Fig. 3 Evaluation of the electrochemical performance of the symmetric device at different total CP masses (0–0.32 g). **a** Cyclic voltammograms of the CFP-CP electrode in a three-electrode setup (scan rate of 1 mV s^{-1}), **b** Cyclic voltammogram of the CFP-CP/separator/CFP-CP symmetric device at a scanning rate of 5 mV sec^{-1} . **c** Galvanostatic charge/discharge curves and the voltage window of 0–1 V in the room temperature (current = 15 mA). **d** Evolution of the charge ratio $[Q(\text{ch})/Q(\text{disch})]$ versus CP masses

sizes coming from activated carbon and carbon black particles; and at the same time a desirable flow-through electrode with low flow resistance in the center of the CP/CFP/CP structured electrode. From now on, for the sake of simplicity, we will call this new architecture for the flow-through electrode as the CFP-CP electrode.

We studied the electrochemical behavior of symmetric CDI devices prepared with identical electrodes. The CV curve of the CFP-CP electrode in a three-electrode setup (Ag/AgCl reference) is recorded at a scan rate of 1 mV sec^{-1} and displays a quasi-rectangular shape attributed to the formation of electric double layers (EDL) at the carbon-electrolyte interface. The capacitive current level is $I = \frac{1}{2} C (\text{dV}/\text{dt})$, with C the capacitance, V the voltage, and t the time. Distortion in the CV curve with an increasing current above 0.6 V indicates the occurrence of faradaic side reactions (Fig. 3a) even though investigated devices operate below the thermodynamic water splitting voltage ($\sim 1.2 \text{ V}$) (Abbas et al. 2018). Note that it is on purpose that we did not want to remove the dissolved gas in the salt solution to see how critical side reactions would be in real desalination applications with those new flow-through electrode designs. The CV curve of the symmetric device (CFP-CP/separator/CFP-CP) was recorded at a scan rate of 5 mV sec^{-1} and displays a similar trend with a strong capacitive contribution and a nonlinear faradaic current contribution (Fig. 3b). Increasing the mass of the CP layer deposited on the carbon fiber paper leads to both an obvious increase in the capacitance as the square box contribution to the cyclic voltammogram is growing, and an enhancement of the faradaic side reaction at 1 V (Fig. 3b). The capacitive current increases with the amount of CP deposited on the CFP electrode since the surface area per volume and thus the capacitance increases.

To further investigate the effect of increasing the thickness of the carbon nanoparticle layer on the carbon fiber paper, galvanostatic charge–discharge (GCD) measurements were taken at a current density of 15 mA and for a voltage window of 0–1 V (Fig. 3c). For an ideal capacitor, the GCD curve is triangular with linear charge and discharge due to the formation of the electric double layer capacitor (EDLC) at the electrode-solution interface. Here, for devices with thick CP layers, the charging process is accompanied with a deviation from the ideal linear increase of voltage versus time. Indeed, the GCD curve displays a shoulder at about 0.6 V that corresponds to the faradaic side reaction (Zhang



et al. 2018). On the discharge curve, this shoulder is not visible as the voltage is set to zero, so the EDLC is quickly discharged, which lowers the electric potential below the potential required for the faradic side reaction. Hence, the ratio between the integrated charges upon charging and discharging [$Q(\text{ch})/Q(\text{disch})$] is larger than 100% because of the current used in the faradic side reaction. Note that the slowest charging processes are found for a mass of CP = 0.16 g while for higher CP masses, the faradic charge decreases upon charging at the same time as the amount of capacitive charge found upon discharging.

In the plot of [$Q(\text{ch})/Q(\text{disch})$] versus the mass of the CP layer, the percentage rises with the mass from 153% at 0 g to 291% at 0.1 g. This implies that the microporous carbon is triggering the side reaction. The suspected side reaction could be the reduction of dissolved oxygen on the negatively charged electrode and the oxidation of the binder on the positive electrode (Xiao et al. 2015). It is indeed found in the literature that activated carbon has some catalytic activity for the oxygen reduction reaction. It appears that the oxygen-containing groups on its surface (carboxylate, ketone, and hydroxyl) could generate some catalytic sites (Watson et al. 2013).

By using the $Q(\text{disch})$ on the GCD curves, we can calculate the evolution of the capacitance versus the mass of the CP deposited on the carbon fiber paper (Fig. 4a). As expected from the CV behavior, the capacitance increases from 0.006 F as the pure CFP (0 g of CP) to 0.35 F when the CFP is loaded with 0.16 g of CP; while higher CP mass leads to a drop in capacitance to 0.2 F at 0.32 g. It is also interesting to look at the data with another viewing angle, by considering the specific capacitance of the CP layer. Normally it should not change by increasing the CP mass as it is a material parameter coupled to the surface area by forming EDLC in the electrolyte. However, we observe that first the specific capacitance increases from 25 to 37 F/g at 0.16 g, reaching a plateau as expected for a constant specific capacitance; but then it significantly diminishes to 10 F/g for 0.32 g (Fig. 4b). This sudden drop suggests that the CP layer cannot be effectively charged due to a resistive effect in the electrode. It is a priori not clear whether this originates from the ionic transport in the porous layer or from the electronic transport in the CFP-CP electrode. We thus analyzed the IR drop versus CP mass (Fig. 4c) and observe the following: the IR drop is large for the CFP alone, while a small addition of carbon particles leads to a decrease in the resistance from 2.2 Ω down to approximately 1.6 Ω at 0.014 g of CP mass. It seems that carbon particles deposited on carbon fibers could ensure better electrical connection with the copper foil in contact with the CFP-CP electrode or that the resistance between the carbon fibers is lowered by the presence of CP particles. A systematic increase in the CP mass leads to a more resistive behavior up to 2.6 Ω

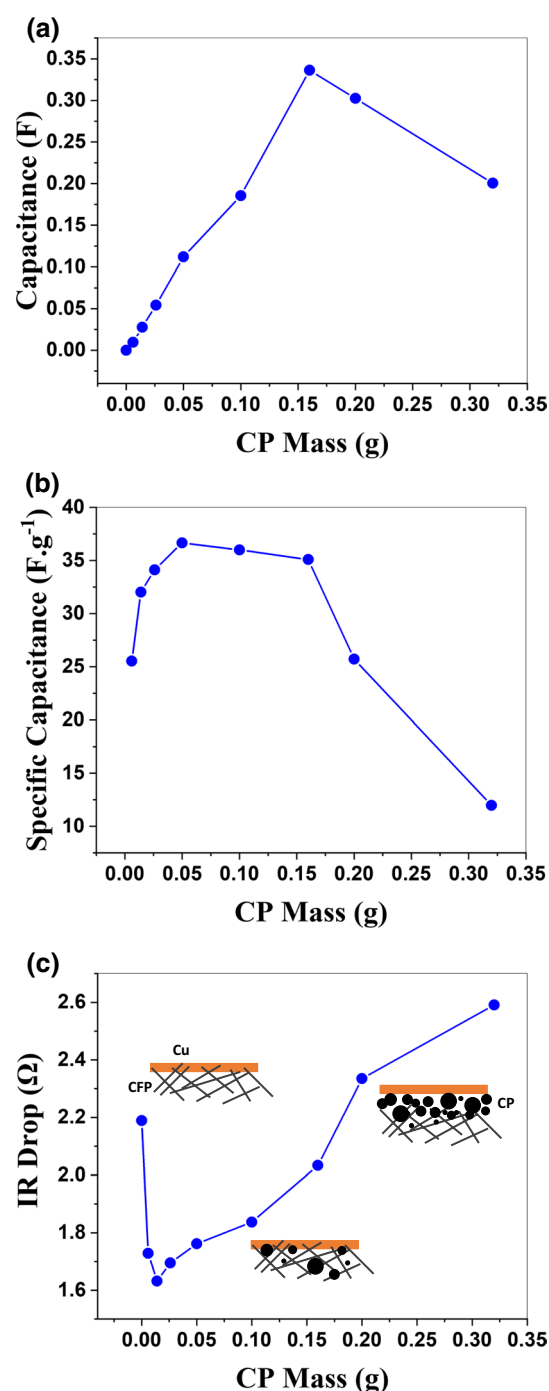


Fig. 4 Evaluation of the electroadsorption performance of the symmetric device at different total CP masses (0–0.32 g). **a** Total capacitance, **b** galvanostatic specific capacitance, and **c** IR drop at 15 mA and the voltage window of 0–1 V at room temperature

at 0.32 g, which is tentatively attributed to the CP layer getting thicker and being a new intermediate layer between the copper electrode and the carbon fiber paper. This evolution of the serial resistance could explain the peculiar behavior observed for (i) the ratio [$Q(\text{ch})/Q(\text{disch})$] getting lower for

high CP mass (Fig. 3d); and (ii) the drop in capacitance for high CP mass. Indeed, both those trends can be affected by the voltage drop across the electrode.

The specific capacitance increased to as high as 37 F/g which is 3193 times higher than that of the device made of the bare hydrophilized CFPs by dropping IR drop. This enhancement indicates the improvement in the conductivity, surface area, and pore morphology leading to more ion transferring at the electrode/electrolyte interface. While the decrease of the specific capacitance, calculated from CV and GCD experiments, by extremely adding CP mass is due to higher internal resistance and thereby a lower utilization efficiency of CP materials resulting in a lower capacitance performance. The specific capacitance increased to as high as 37 F/g which is 3193 times higher than that of the device made of the bare hydrophilized CFPs by dropping IR drop. This enhancement indicates the improvement in the conductivity, surface area, and pore morphology leading to more ion transferring at the electrode/electrolyte interface. While the decrease of the specific capacitance, calculated from CV and GCD experiments, by extremely adding CP mass is due to higher internal resistance and thereby a lower utilization efficiency of CP materials resulting in a lower capacitance performance.

We need to characterize CFP-CP devices by electrochemical impedance spectroscopy (EIS), which hopefully can reveal other hidden phenomena and separate the contribution response of solution resistance, charge transfer resistance, double layer capacitance, and other physiochemical processes in this symmetric charge storage system. Figure 5 reports the Nyquist and Bode plots of symmetrical devices with various CP masses. The small AC signal (5 mV) is applied on the symmetric device CFP-CP/separator/CFP-CP over a frequency range from 100 to 200 kHz. The Nyquist plot is depicted in Fig. 5a and displays for the CFP (0 g of CP) a tilted line crossing the X-axis at nonzero value. This crossing indicates a resistance at high frequency and the almost vertical line is the result of a strong capacitive character at low frequency. Now, by zooming on the inset of Fig. 5a, it is also possible to see a partial semicircle that indicates that in addition to a capacitor in series with a resistor, there must be a resistive component in parallel with the capacitor. We observe that the larger the CP mass, the more vertical is the tail in the Nyquist plot which suggests some modification in the diffusive transport of the ions (which could be modeled by a Warburg element). The Bode plot of the carbon fiber paper (0 g of CP) in Fig. 5b reveals several frequency regions: (i) at high frequency (> 100 kHz), there is a measurement artifact inducing a positive phase angle that can be simulated with an inductance (Cooper et al. 2017); (ii) between 1 and 100 kHz, the phase angle is close to zero and thus the impedance has a strong resistive character, which could be either ionic transport in the

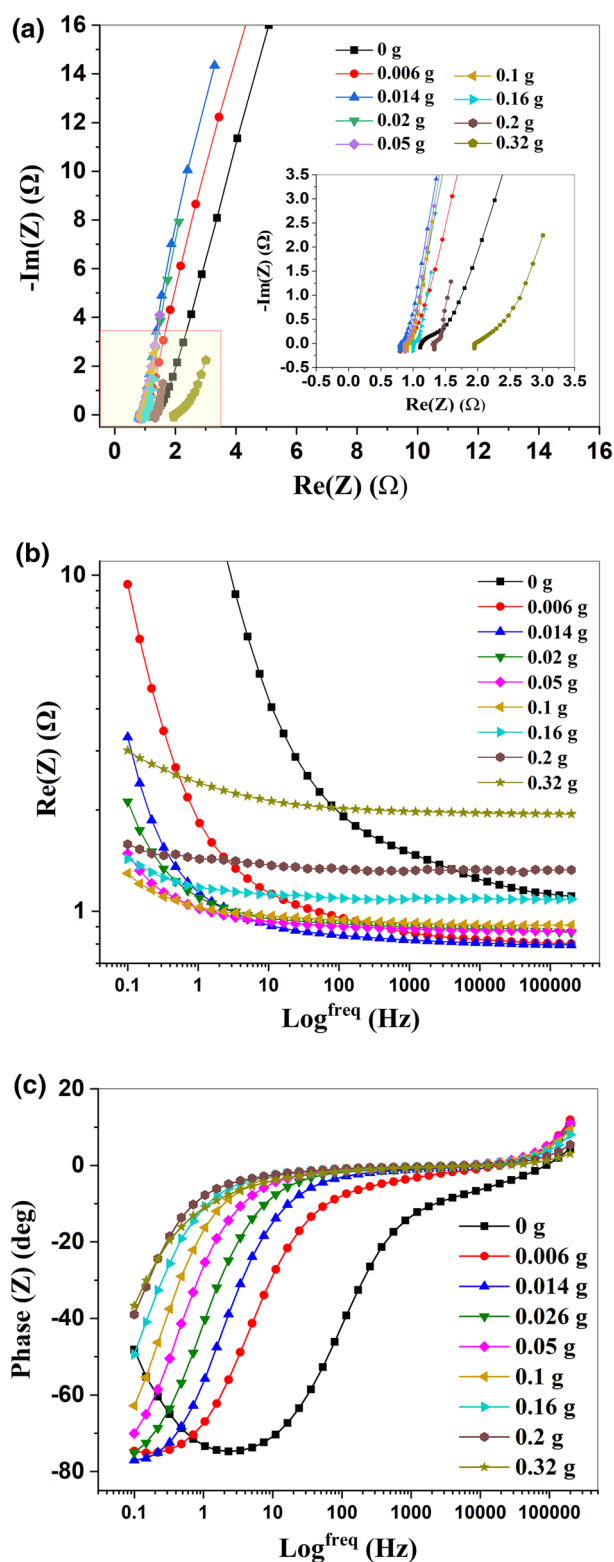
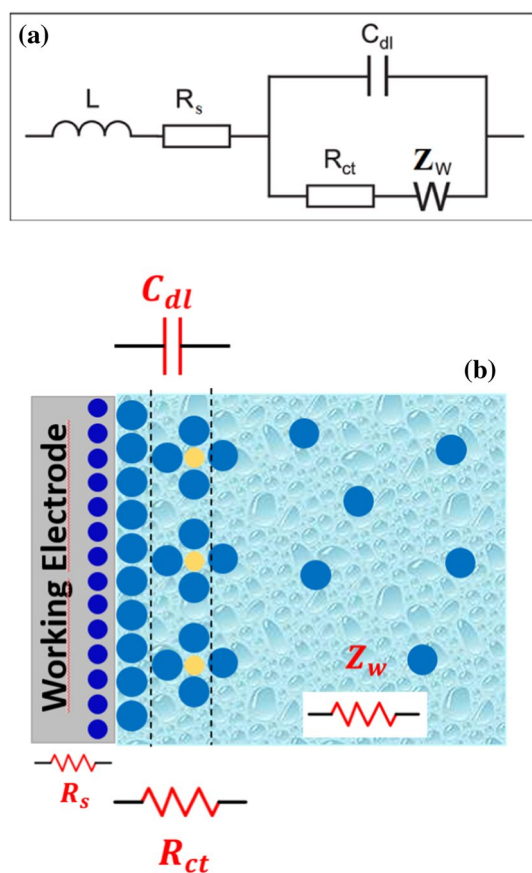


Fig. 5 Evaluation of the electrochemical impedance performance of the symmetric devices at different total CP masses (0–0.32 g). **a** Nyquist plot, **b** phase angle versus frequency, and **c** real part of the impedance versus frequency

electrolyte or electronic transport in the electrode; (iii) then a capacitive region with a phase angle close to -90° in the frequency range [0.1–100 Hz], (iv) finally a low frequency a new trend of a slight emerging a resistive behavior which could be potentially coupled to a faradic side reaction, i.e., a charge transfer from the electrode to a reactant (which could be modeled by an extra resistance R_{CT}). By increasing the thickness of the CP layer, the spectra are like systematically shifted to lower frequencies but the main behavior remains. Hence, we believe that it should be possible to find an equivalent circuit that can be used to fit all the experimental results and extract some trends. The proposed circuit is depicted in Scheme 1.

The results of the fitting of the impedance spectra with the equivalent circuit are visualized in the supplementary information. The model is rather simple for a porous electrode. We have tried several more complex transfer line models but without much success, i.e., some parameters lost their physical meaning, and even if the fitting is good the physical



Scheme 1 Schematics of **a** a designed simulated circuit with the presence of **b** elements in the electrode/electrolyte interface. Ohmic resistance of the electrolyte solution between the working electrode and the counter electrode (R_s), the double layer capacitance (C_{DL}), the charge transfer resistance of electrodes (R_{CT}), Warburg impedance (Z_w), and electrode inductance (L)

meaning of the TLM equivalent circuit is discussable (Barbero and Lelidis 2017). Hence, we believe the simple equivalent circuit is good enough to identify the basic physical phenomena as indicated by the following comparison: the IR drop extracted from GCD curves follows the same trend as the serial resistance R_{ESR} for various CP mass and are the about 1 to 2 Ω (Fig. 6a). Moreover, the capacitance extracted

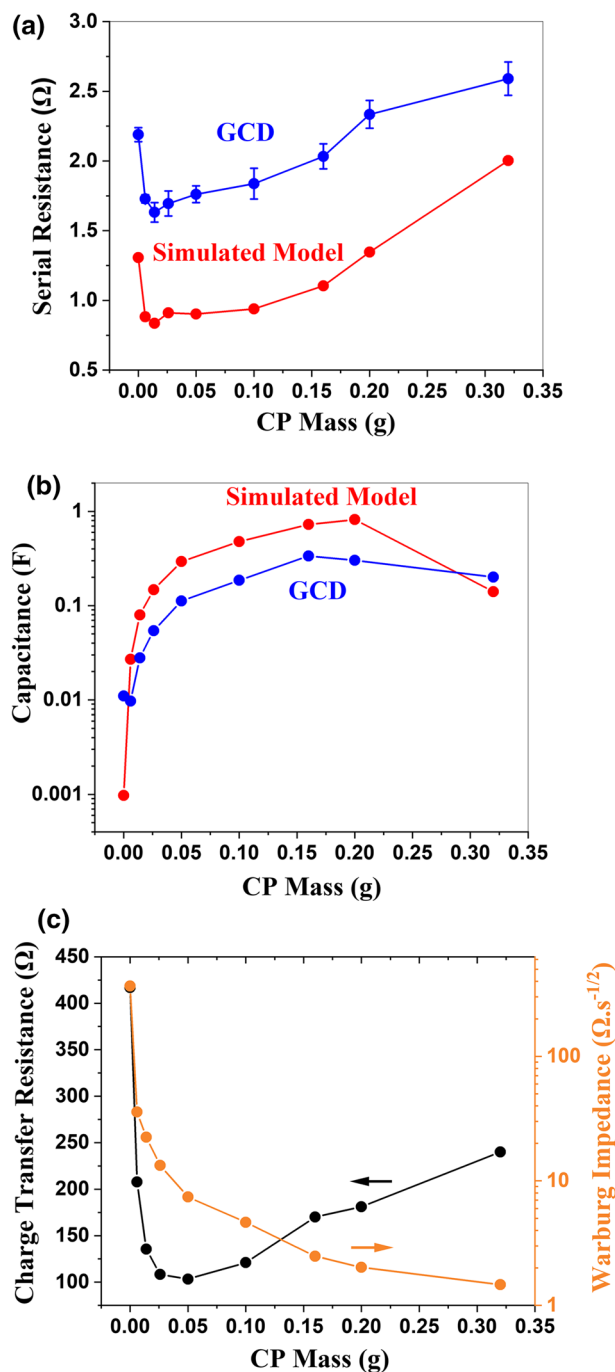


Fig. 6 Comparing of **a** the serial resistance, **b** capacitance, and **c** charge transfer resistance achieved by equivalent circuit and results from the GCD at different CP masses

from GCD curves and the C_{DL} in the circuit follows a similar trend versus the CP mass and their values are not far away from each other. We found that the capacitance from the GCD likely underestimates a bit the real value of the C_{DL} except for the lowest and highest CP masses related to less fitting the simulated data to the experimental data. The advantages of the impedance spectroscopy technique arise when the equivalent circuits make sense and that other hidden components such as the Warburg component and the charge transfer resistance are extracted by the fitting procedure. R_{CT} value of the carbon fiber paper is about 416 Ω and it decreases to 103 Ω for 0.05 g, after the thicker CP layer, the charge transfer resistance increases to 240 Ω at 0.32 g. It is notable that the R_{ESR} is 2 orders of magnitude smaller than the R_{CT} . This is the reason why we believe that R_{CT} represents a resistive mechanism with a higher relaxation time than electronic transport, potentially an electron transfer of a low kinetic constant related to a faradic side reaction. But R_{CT} like R_{ESR} are actually following the same trend and its values stay within the same order of magnitude when increasing the CP mass, while C_{DL} is increased by three orders of magnitude. Besides the capacitance, one more element is significantly varying and this is the Warburg component, diminishing from ~ 365 to $\sim 3 \Omega s^{-1/2}$, i.e., dropping by two orders of magnitude (Fig. 6c). We tentatively explain this large drop to the change in the electrode geometry while adding the carbon particles on the CFP. Starting from the carbon fiber paper, the micrometer size fibers are expected to lead to a “microelectrode effect” where the mass diffusion is promoted in three dimensions. On the contrary, when the CP layer is added it goes from a 3D diffusion effect to a more 2D diffusion because of the coating of the CP layer, which also includes a tortuosity effect for the ion diffusion. Hence, the addition of the CP mass actually changes dramatically the diffusion regime for the ions upon charging the electrode.

Conclusion

A low-cost and easy manufactured flow-through electrode is proposed by depositing a slurry of microporous carbon particles on top of the microporous carbon fiber paper. We built a symmetric device made of two similar flow-through electrodes separated by a separator in brackish water. We have demonstrated that the addition of the CP slurry leads to an increase of 3 orders of magnitude in capacitance for the device, while the electrode and the device have an open structure that should enable easy fluid dynamics. Hence, this architecture seems promising for electrochemical flow cells used in capacitive desalination or electrolysis reactor.

By testing with non-degassed NaCl electrolyte to simulate the situation for simple desalination, it appears that the activated carbon particles trigger a faradic reaction already

at 0.6 V, which is attributed to the oxygen reduction reaction. This is an important effect to take into consideration when using those flow-through electrodes for various applications. This side reaction is also identified in impedance spectroscopy as charge transfer resistance. The impedance spectroscopy analysis with a simple model enables us to decouple several phenomena in the time domains. The diffusion part of the spectra is significantly changed as is expected from the completely different situation for the ion diffusion going from a 3D network of microfibers to a planar coating of microporous conducting particles. As the next step, we will evaluate the flow-through electrodes including the dynamic flow of the fluid.

Acknowledgements This work was financially supported by the Swedish Research Council (VR 2016-05990), the Knut and Alice Wallenberg Foundation (KAW 2018.0058), the Swedish Energy Agency (P52023-1), and the Swedish Government Strategic Research Area in Materials Science on Advanced Functional Materials at Linköping University (Faculty Grant SFO-Mat-LiU No. 2009-00971).

Funding Open access funding provided by Linköping University.

Declarations

Conflict of interest The authors declare that they have no conflict of interest.

Open Access This article is licensed under a Creative Commons Attribution 4.0 International License, which permits use, sharing, adaptation, distribution and reproduction in any medium or format, as long as you give appropriate credit to the original author(s) and the source, provide a link to the Creative Commons licence, and indicate if changes were made. The images or other third party material in this article are included in the article's Creative Commons licence, unless indicated otherwise in a credit line to the material. If material is not included in the article's Creative Commons licence and your intended use is not permitted by statutory regulation or exceeds the permitted use, you will need to obtain permission directly from the copyright holder. To view a copy of this licence, visit <http://creativecommons.org/licenses/by/4.0/>.

References

- Abbas S, Lee H, Hwang J, Mehmood A, Shin HJ, Mehboob S, Lee JY, Ha HY (2018) A novel approach for forming carbon nanorods on the surface of carbon felt electrode by catalytic etching for high-performance vanadium redox flow battery. *Carbon* 128:31–37. <https://doi.org/10.1016/j.carbon.2017.11.066>
- Alkhadra MA, Su X, Suss ME, Tian H, Guyes EN, Shocron AN, Bazant MZ (2022) Electrochemical methods for water purification, ion separations, and energy conversion. *Chem Rev* 122:13547–13635. <https://doi.org/10.1021/acs.chemrev.1c00396>
- Barbero G, Lelidis I (2017) Analysis of Warburg's impedance and its equivalent electric circuits. *Phys Chem Chem Phys* 19:24934–24944. <https://doi.org/10.1039/C7CP04032F>
- Bengoa C, Montillet A, Legentilhomme P, Legrand J (1997) Flow visualization and modelling of a filter-press type electrochemical reactor. *J Appl Electrochem* 27:1313–1322. <https://doi.org/10.1023/A:1018456609059>

- Chander S, Mangal M (2019) Electrochemical properties of different carbon nano materials. *BICON*. <https://doi.org/10.1149/1.2868772>
- Chmiola J, Yushin G, Dash R, Gogotsi Y (2006) Effect of pore size and surface area of carbide derived carbons on specific capacitance. *J Power Sources* 158:765–772. <https://doi.org/10.1016/j.jpowsour.2005.09.008>
- Cooper SJ, Bertei A, Finegan DP, Brandon NP (2017) Simulated impedance of diffusion in porous media. *Electrochim Acta* 251:681–689. <https://doi.org/10.1016/j.electacta.2017.07.152>
- Eijkelkamp N, Linley JE, Torres JM, Bee L, Dickenson AH, Gringhuis M, Minett MS, Hong GS, Lee E, Oh U, Ishikawa Y, Zwartkuis FJ, Cox JJ, Wood JN (2013) A role for Piezo₂ in EPAC1-dependent mechanical allodynia. *Nat Commun* 4:1–13. <https://doi.org/10.1038/ncomms2673>
- Elgrishi N, Rountree KJ, McCarthy BD, Rountree ES, EisenhartLDempsey TTJ (2018) A practical beginner's guide to cyclic voltammetry. *J Chem Educ* 95:197–206. <https://doi.org/10.1021/acs.jchemed.7b00361>
- Elisadiki J, King'ondou CK (2020) Performance of ion intercalation materials in capacitive deionization/electrochemical deionization: a review. *J Electroanal Chem* 878:114588. <https://doi.org/10.1016/j.jelechem.2020.114588>
- Epstein N (1989) On tortuosity and the tortuosity factor in flow and diffusion through porous media. *Chem Eng Sci* 44:777–779. [https://doi.org/10.1016/0009-2509\(89\)85053-5](https://doi.org/10.1016/0009-2509(89)85053-5)
- Fedorov MV, Kornyshev AA (2008) Ionic liquid near a charged wall: structure and capacitance of electrical double layer. *J Phys Chem B* 112:11868–11872. <https://doi.org/10.1021/jp803440q>
- Merlet C, Rotenberg B, Madden PA, Taberna PL, Simon P, Gogotsi Y, Salanne M (2012) On the molecular origin of supercapacitance in nanoporous carbon electrodes. *Nat Mater* 11:306–310. <https://doi.org/10.1038/nmat3260>
- Mo Y, Lu Z, Rughoobur G, Patil P, Gershenfeld N, Akinwande AI, BuchwaldJensen SLKF (2020) Microfluidic electrochemistry for single-electron transfer redox-neutral reactions. *Science* 368:1352–1357. <https://doi.org/10.1126/science.aba3823>
- Olabi AG, Abbas Q, Al Makky A, Abdelkareem MA (2022) Supercapacitors as next generation energy storage devices: properties and application. *Energy* 248:123617. <https://doi.org/10.1016/j.energy.2022.123617>
- Pean C, Daffos B, Rotenberg B, Levitz P, Haefele M, Taberna PL, Simon P, Salanne M (2015) Confinement, desolvation, and electrosorption effects on the diffusion of ions in nanoporous carbon electrodes. *J Am Chem Soc* 137:12627–12632. <https://doi.org/10.1021/jacs.5b07416>
- Porada S, Zhao R, Van der Wal A, Presser V, Biesheuvel PM (2013) Review on the science and technology of water desalination by capacitive deionization. *Prog Mater Sci* 58:1388–1442. <https://doi.org/10.1016/j.pmatsci.2013.03.005>
- Ribadeneyra MC, Grogan L, Au H, Schlee P, Herou S, Neville T, Cullen PL, Kok MDR, Hosseinaei O, Danielsson S, Tomani P, Titirici MM, Brett DJL, Shearing PR, Jervis R, Belen Jorge A (2020) Lignin-derived electrospun freestanding carbons as alternative electrodes for redox flow batteries. *Carbon* 157:847–856. <https://doi.org/10.1016/j.carbon.2019.11.015>
- Rivera FF, De León CP, Nava JL, Walsh FC (2015) The filter-press FM01-LC laboratory flow reactor and its applications. *Electrochim Acta* 163:338–354. <https://doi.org/10.1016/j.electacta.2015.02.179>
- Suss ME, Baumann TF, Bourcier WL, Spadaccini CM, Rose KA, Santiago JG, Stadermann M (2012) Capacitive desalination with flow-through electrodes. *Energy Environ Sci* 5:9511–9519. <https://doi.org/10.1039/C2EE21498A>
- Tröltzsch U, Kanoun O (2012) Generalization of transmission line models for deriving the impedance of diffusion and porous media. *Electrochim Acta* 75:347–356. <https://doi.org/10.1016/j.electacta.2012.05.014>
- Volonino L, Robinson S, Watson HJ (1992) EIS and organizational change. In: Jelassi T, Klein MR, Mayon-White WM (eds) Decision support systems: experiences and expectations. North-Holland, p 309–321. <https://doi.org/10.1016/B978-0-444-89673-5.50028-8>
- Watson VJ, Nieto Delgado C, Logan BE (2013) Influence of chemical and physical properties of activated carbon powders on oxygen reduction and microbial fuel cell performance. *Environ Sci Technol* 47:6704–6710. <https://doi.org/10.1021/es401722j>
- Xiao H, Wu M, Zhao G (2015) Electrocatalytic oxidation of cellulose to gluconate on carbon aerogel supported gold nanoparticles anode in alkaline medium. *Catalysts* 6:5. <https://doi.org/10.3390/catal6010005>
- Zhang W, Xi J, Li Z, Zhou H, Liu L, Wu Z, Qiu X (2013) Electrochemical activation of graphite felt electrode for VO₂⁺/VO₂⁺ redox couple application. *Electrochim Acta* 89:429–435. <https://doi.org/10.1016/j.electacta.2012.11.072>
- Zhang X, Zuo K, Zhang X, Zhang CH, Liang P (2018) Selective ion separation by capacitive deionization (CDI) based technologies: a state-of-the-art review. *Environ Sci Water Res Technol* 6:243–257. <https://doi.org/10.1039/C9EW00835G>

Publisher's Note Springer Nature remains neutral with regard to jurisdictional claims in published maps and institutional affiliations.